Cancer Letters 644 (2026) 218311

Contents lists available at ScienceDirect

Cancer Letters

journal homepage: www.elsevier.com/locate/canlet

Original Articles

SLC5A11 mediates metformin-induced PD-L1 suppression to enhance cancer immunotherapy through AMPK–IRF1 signaling

Yarui Ma [a,1], Xue Wang [a,1], Zhewen Wei [b,1], Qi Zhang [a,1], Fangqing Yuan [a], Chungui Xu [a], Chang Liu [c,d], Xiaobing Wang [a,*], Lin Li [e,**], Yuchen Jiao [a,f,***]

[a] State Key Laboratory of Molecular Oncology, National Cancer Center/National Clinical Research Center for Cancer/Cancer Hospital, Chinese Academy of Medical Sciences and Peking Union Medical College, 100021, Beijing, China
[b] Department of Hepatobiliary Surgery, National Cancer Center/National Clinical Research Center for Cancer/Cancer Hospital, Chinese Academy of Medical Sciences and Peking Union Medical College, Beijing, China
[c] Amsterdam UMC location Vrije Universiteit Amsterdam, Pulmonary Medicine, De Boelelaan, 1117, Amsterdam, the Netherlands
[d] Amsterdam Institute for Infection and Immunity, Cancer Center Amsterdam, Amsterdam, the Netherlands
[e] Department of Medical Oncology, Beijing Hospital, National Center of Gerontology, Institute of Geriatric Medicine, Chinese Academy of Medical Sciences, Beijing, 100730, China
[f] Institute of Cancer Research, Henan Academy of Innovations in Medical Science, Zhengzhou, Henan, China

ARTICLE INFO

Keywords:
CRISPR screen
Metformin
SLC5A11
PD-L1
Immune checkpoint blockade

ABSTRACT

Metformin exhibits immunomodulatory properties in cancer treatment, but the underlying mechanisms remain elusive. Using genome-wide CRISPR screening, we identified SLC5A11 as an essential mediator of metformin sensitivity. Molecular docking and dynamics simulations revealed direct metformin-SLC5A11 binding at the pocket containing Asn78 and Glu102 residues. Metformin suppressed PD-L1 expression across multiple cancer models through SLC5A11-dependent activation of AMPK and subsequent JAK2-STAT1-IRF1 downregulation. SLC5A11 knockout abolished these effects, while reconstitution restored metformin responsiveness. In syngeneic mouse models of lung and pancreatic cancer, combining metformin with anti-PD1 therapy produced synergistic antitumor effects, enhanced T cell infiltration, and potentiated immunotherapy efficacy. Metformin pretreatment significantly enhanced PBMC-mediated cytotoxicity against tumor cells and patient-derived organoids in ex vivo co-culture systems. Our findings establish the SLC5A11-AMPK-PD-L1 axis as a novel mechanism linking metformin to tumor immunity, providing a molecular rationale for combining metformin with checkpoint inhibitors in cancer immunotherapy.

1. Introduction

Metformin, the first-line antidiabetic drug, has emerged as a promising anticancer agent. Epidemiological studies demonstrate that metformin use correlates with reduced cancer incidence and improved outcomes across multiple malignancies [1,2]. Beyond direct antitumor effects through AMPK activation and metabolic reprogramming [3], recent evidence reveals metformin's profound immunomodulatory properties. Metformin enhances cytotoxic $CD8^+$ T lymphocyte infiltration and function while suppressing regulatory T cells and myeloid-derived suppressor cells [4–7], reverses T cell exhaustion [8,9], and improves responses to immune checkpoint inhibitors in preclinical settings [5,10]. However, the molecular mechanisms underlying these immunomodulatory effects remain incompletely understood.

A critical gap exists in understanding how metformin interfaces with cellular machinery to modulate tumor immunity. While organic cation transporters mediate metformin uptake [11], the specific molecular interactions governing its effects on immune checkpoint expression remain undefined. Recent studies highlight the importance of solute carrier (SLC) transporters in cancer metabolism and immunity [12–16].

* Corresponding author.
** Corresponding author.
*** Corresponding author. State Key Laboratory of Molecular Oncology, National Cancer Center/National Clinical Research Center for Cancer/Cancer Hospital, Chinese Academy of Medical Sciences and Peking Union Medical College, 100021, Beijing, China.
E-mail address: jiaoyuchen@cicams.ac.cn (Y. Jiao).
[1] Contributed equally.

https://doi.org/10.1016/j.canlet.2026.218311
Received 7 August 2025; Received in revised form 23 January 2026; Accepted 7 February 2026
Available online 12 February 2026

Among these, SLC5A11, a sodium/glucose cotransporter, participates in metabolic homeostasis and tumor progression [14], though its role in immune regulation remains unexplored. Given metformin's effects on cellular metabolism and emerging evidence of its ability to modulate PD-L1 expression [17,18], we hypothesized that specific metabolic transporters might mediate metformin's immunomodulatory effects.

In this study, we employed an unbiased genome-wide CRISPR screen to identify molecular determinants of metformin cytotoxicity in cancer cells. This approach led to the unexpected discovery of SLC5A11 as a critical mediator of metformin-induced cytotoxicity and immunomodulation. We demonstrate that metformin directly binds to SLC5A11 and is required for metformin's ability to suppress PD-L1 expression through a novel AMPK-JAK2-STAT1-IRF1 signaling axis. Moreover, combining metformin with immune checkpoint blockade produces synergistic antitumor effects in preclinical models, including immunotherapy-resistant pancreatic cancer. These discoveries establish SLC5A11 as a previously unrecognized target of metformin and provide a molecular framework for rationally combining metabolic interventions with cancer immunotherapy.

2. Results

2.1. CRISPR-Cas9 screening identifies SLC5A11 as a critical mediator of metformin cytotoxicity

Given the emerging evidence for metformin's anticancer properties yet incomplete understanding of its molecular targets, we sought to systematically identify genes essential for metformin-induced cytotoxicity. We performed a genome-wide CRISPR/Cas9 knockout screening using the Brunello library comprising 76,441 sgRNAs targeting 19,114 genes in U251-MG glioblastoma cells. Following lentiviral transduction and puromycin selection, cells were subjected to continuous metformin treatment (5 mM) for 14 days, thereby creating strong selection pressure for sgRNAs that conferred resistance to metformin-induced cytotoxicity (Fig. 1A). Genomic DNA extracted from surviving cell populations was subjected to next-generation sequencing and analyzed using the MAGeCK algorithm to identify significantly enriched sgRNAs. This analysis revealed 1001 candidate genes whose deletion significantly enhanced cell survival under metformin selection ($p < 0.05$), representing potential mediators of metformin sensitivity (Fig. 1B). Among the top 10 most significantly enriched genes, we prioritized SLC5A11 (Solute Carrier Family 5 Member 11) for further functional validation based on its established role in cellular metabolism and endoplasmic reticulum dynamics (Fig. 1C).

To validate our screening findings, we generated stable SLC5A11-knockout (SLC5A11-KO) cell lines using CRISPR/Cas9 and assessed their sensitivity to metformin (Supplementary Fig. S1A). Consistent with our screening results, knockout of SLC5A11 conferred marked resistance to metformin-induced growth inhibition across a range of concentrations (Fig. 1D). These findings establish SLC5A11 as a critical determinant of cellular cytotoxicity to metformin and implicate this transporter as an important component of metformin's anticancer effects.

2.2. Metformin physically interacts with SLC5A11 by molecular modeling

Given SLC5A11's role as a sodium/glucose symporter, we hypothesized that it might directly interact with metformin to mediate its cellular effects. To test this hypothesis, we employed molecular docking simulations to predict potential binding interactions between metformin and the SLC5A11 protein structure. Our computational analysis identified 20 potential binding conformations distributed across three distinct binding pockets within the SLC5A11 structure (Supplementary Fig. S2A). The binding affinity of metformin to SLC5A11 was comparable to that of previously validated metformin-binding proteins such as PEN2 and SLC22A1 (Supplementary Tables S1–3 and Supplementary Fig. S2B and C) [19,20]. Detailed analysis of the highest-ranked binding conformations within each pocket revealed distinct interaction patterns: in binding site 1, metformin formed hydrogen bonds with Val338 (3.09 Å), Cys340 (3.32 Å), Ser354 (2.91 Å), Cys356 (3.13 Å), Cly444 (3.02 Å), complemented by hydrophobic interactions with Ala93, Arg331, Ala339, Gly355, Ser357, Gly445, and Gln446. At binding site 2, metformin established critical hydrogen bonds with Asn78 (3.15 Å) and Glu102 (3.09 Å), along with hydrophobic interactions with Tyr101, Ser282, Tyr285, Phe448, and Gln452. In binding site 3, metformin formed hydrogen bonds with Asp498 (3.19 Å) and Tyr501 (2.91 Å), supported by hydrophobic interactions with Ser442, Tyr450, Ser453, Val502, and Gln503 (Fig. 1E–G and Supplementary Fig. S2D–F).

To evaluate the stability of these protein-ligand interactions, we performed 100-ns molecular dynamics (MD) simulations on each highest-ranked metformin-SLC5A11 complex. The root mean square deviation (RMSD) analysis revealed that all three complexes rapidly achieved conformational stability within 20 ns and maintained stable configurations throughout the remaining simulation period (Fig. 1H). The RMSD values of the three complexes rapidly stabilized at 1.02 ± 0.46 nm, 1.02 ± 0.25 nm, and 0.98 ± 0.60 nm, respectively (Fig. 1H). The root mean square fluctuation (RMSF) analysis indicated relatively high overall protein flexibility (Fig. 1I). Importantly, hydrogen bond analysis demonstrated that only the metformin-site 2 complex maintained stable hydrogen bonding throughout the simulation period, in contrast to the transient interactions observed at sites 1 and 3 (Fig. 1J). The binding free energies (ΔGbind) calculations using the MM/GBSA method corroborated the preferential binding at site 2, with site 3 (−11.21 kcal/mol) < site 1 (−29.69 kcal/mol) < site 2 (−34.45 kcal/mol) (Fig. 1K). The substantially more favorable binding energy of the site 2 interaction, coupled with its hydrogen bond stability during MD simulation, strongly suggests that metformin preferentially interacts with SLC5A11 at the binding pocket containing the critical Asn78 and Glu102 residues.

To assess whether this binding preference is conserved across species, we first performed a protein sequence alignment between human SLC5A11 and mouse Slc5a11 using Clustal Omega (https://www.ebi.ac.uk/jdispatcher/msa/clustalo). The analysis revealed that human and mouse SLC5A11 share 86.48% sequence identity, indicating a high degree of evolutionary conservation across the full-length protein. We further performed molecular docking analysis at the corresponding site in mouse Slc5a11. Consistent with the human data, metformin exhibited comparable binding affinities and a similar interaction pattern at mouse site 2 (Supplementary Fig. S2G). These results support the evolutionary conservation of the metformin–SLC5A11 interaction and validate the relevance of the mouse model used in this study.

To validate these computational predictions experimentally, confocal imaging revealed the colocalization of metformin with SLC5A11 in U251-MG cells (Fig. 1L). To validate metformin-SLC5A11 interaction in a cellular context, we performed cellular thermal shift assays (CETSA). Metformin treatment (5 mM, 2 h) significantly increased SLC5A11 thermal stability, with Tm values shifting from 50.78 °C (95% CI: 47.47–52.38) (vehicle) to 57.20 °C (95% CI: 55.28–60.41) (metformin), representing a ΔTm of 6.42 °C ($p < 0.05$, Supplementary Fig. S2H). Quantitative analysis of thermal stability curves revealed significantly higher SLC5A11 levels in metformin-treated cells across the 50 °C – 60 °C temperature range ($p < 0.01$, Supplementary Fig. S2H), providing direct evidence for ligand-induced protein stabilization.

Collectively, these findings provide the structural basis for a direct physical interaction between metformin and SLC5A11, offering a molecular explanation for the essential role of this transporter in metformin sensitivity.

2.3. SLC5A11 is essential for metformin-induced PD-L1 transcriptional downregulation

To comprehensively characterize the transcription changes induced

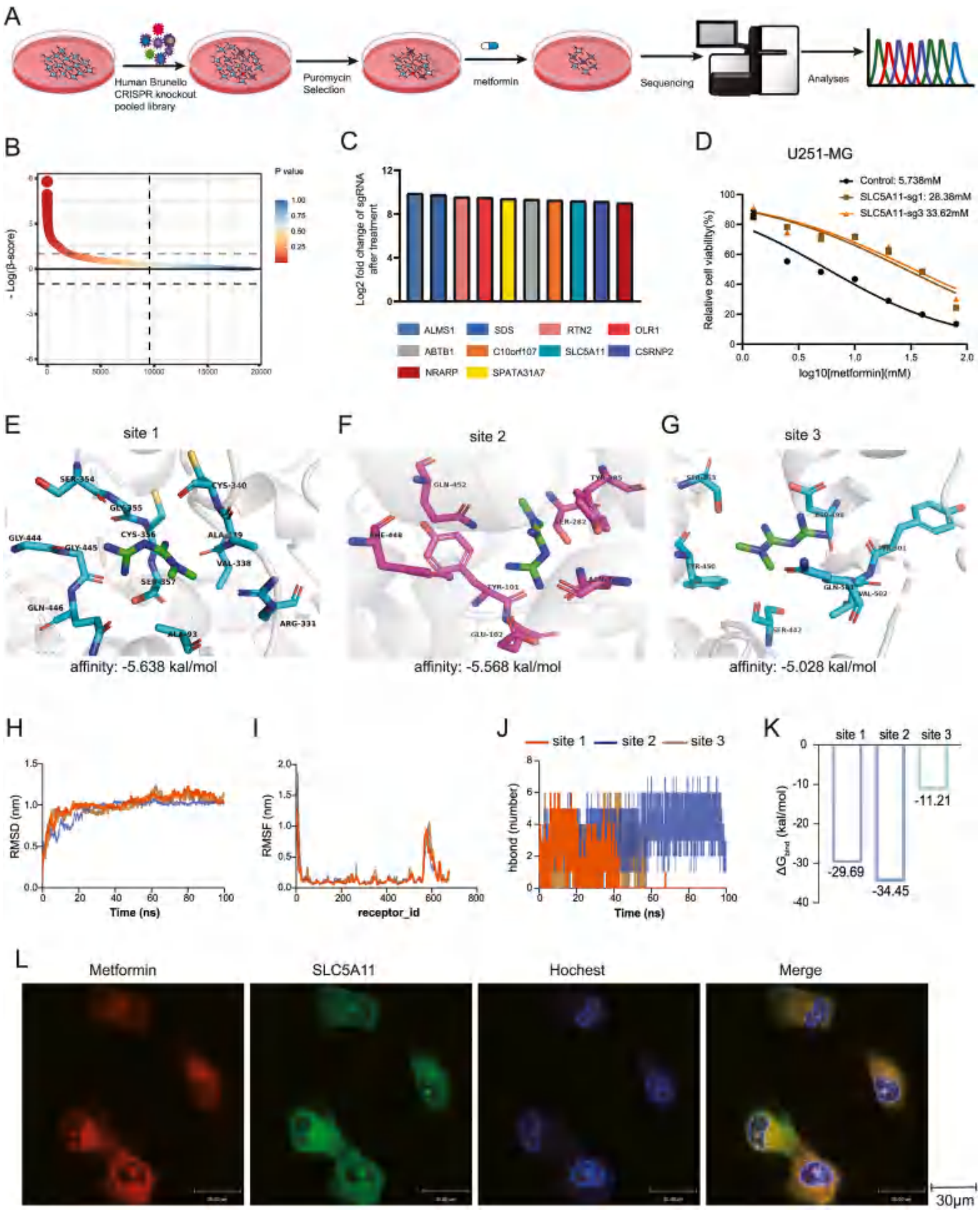

(caption on next page)

Fig. 1. SLC5A11 is the key regulator of metformin
(A) CRISPR-Cas9 functional screening schematic diagram. (B) Genes highly enriched after 14 days treatment of metformin by evaluating the sequencing results in MAGeCK. (C) Histogram of the first 10 differential genes after metformin treatment. (D) Cell viability assessed using the CCK8 test for U251-MG cells in DMEM containing varying concentrations of metformin with knockout of SLC5A11. (E-G) Schematic diagram of the molecular docking between metformin and SLC5A11, and the binding conformation with the highest binding power of the three binding regions is enlarged. (H-J) Molecular dynamics simulation results of the conformation with the highest binding force in the three binding regions: (H) The results of the root mean square deviation (RMSD); (I) The results of the root mean square fluctuation (RMSF); (J) The result of the distribution of hydrogen bonds. (K) Binding free energies (ΔGbind) of the three protein–ligand complexes. (L) Co-localization of SLC5A11 (green) and metformin (red) in U251-MG-SLC5A11-reconstituted cells, cells were infected pLV3-CMV-SLC5A11(human)-3 × FLAG-EF1a-CopGFP-Neo plasmid, then treated with CY5-metformin (1 mM) for 24 h, Scale bars: 30 μm. Results are presented as the mean ± SD. Data are derived from three independent experiments with similar results. (For interpretation of the references to color in this figure legend, the reader is referred to the Web version of this article.)

by metformin, we performed RNA-sequencing analysis comparing U251-MG cells exposed to 5 mM metformin or PBS for 72 h. Gene Set Enrichment Analysis (GSEA) revealed significant difference in multiple immune-regulatory pathways, most notably a striking suppression of PD-L1 expression and PD-1 checkpoint signaling in metformin-treated cells (Fig. 2A). We validated this finding using quantitative RT-PCR analysis, which confirmed significant metformin-mediated suppression of *CD274* transcription across multiple models: glioblastoma (U251-MG), pancreatic ductal adenocarcinoma (K210, derived from LSL-KrasG12D; Trp53 fl/fl; Pdx1-Cre mice), and Lewis lung carcinoma (LLC) (Fig. 2B). Consistent with the transcriptional data, Western blot analyses demonstrated significant reduction of PD-L1 protein levels following metformin treatment in all three cell lines (Fig. 2C–E and Supplementary Fig. S3A–C), establishing a consistent inhibitory effect on PD-L1 expression at both transcriptional and post-translational levels across multiple cancer types. To determine whether this effect extends to the in vivo setting, immunohistochemical staining of tumor xenografts confirmed significantly attenuated PD-L1 expression in metformin-treated specimens compared to vehicle controls (Fig. 2F).

To determine whether SLC5A11 mediates this immunomodulatory effect of metformin, we generated stable SLC5A11 knockout (SLC5A11-KO) cell lines in U251-MG, K210, and LLC cells using CRISPR/Cas9 (Supplementary Fig. S1A–C). Strikingly, genetic ablation of SLC5A11 completely abolished metformin-induced PD-L1 downregulation in all three cancer models, even at high metformin concentrations (5 mM) and extended exposure times (72 h) (Fig. 2G–I and Supplementary Fig. S3D–F). To confirm the specificity of this effect, reconstitution of wild-type SLC5A11 in U251-MG-SLC5A11-KO cells restored metformin's ability to suppress PD-L1 (Fig. 2J, Supplementary Fig. S3G and Supplementary Fig. S4A), confirming the specific requirement for SLC5A11 in this regulatory mechanism. To establish the structural basis for this functional relationship, we leveraged our molecular docking results to engineer SLC5A11 variants with point mutations at predicted metformin binding sites. We generated SLC5A11-KO cells reconstituted with either N78A or E102A SLC5A11 mutations - targeting residues identified as critical for hydrogen bonding with metformin at binding site 2. Remarkably, metformin failed to suppress PD-L1 expression in cells expressing either mutant form of SLC5A11, despite protein levels comparable to wild-type reconstitution (Fig. 2K and L, Supplementary Fig. S3H–I and Supplementary Fig. S4A). These structure-function analyses demonstrate that specific molecular interactions between metformin and SLC5A11, particularly those involving Asn78 and Glu102 residues, are essential for metformin-mediated PD-L1 downregulation. Thus, our data establish a previously unknown role for SLC5A11 as the molecular gateway through which metformin exerts its immunomodulatory effects on tumor cells.

2.4. Metformin suppresses PD-L1 transcription via an IRF1-dependent mechanism

Next, we sought to identify the downstream transcription factors that link SLC5A11 activation to PD-L1 suppression [21]. We analyzed our RNA-sequencing data for differentially expressed transcription factors known to regulate *CD274* transcription. This analysis revealed significant downregulation of multiple transcriptional regulators, including *IRF1*, *MYC*, *BRD4* and *JUN* in metformin-treated U251-MG cells ($|\log2FC| \geq 1$ and $p < 0.05$, Fig. 3A and B). Quantitative RT-PCR validation confirmed the differential expression of these candidate genes, demonstrating that *IRF1* exhibited the most profound down-regulation following metformin treatment ($p < 0.0001$, Fig. 3C). Meanwhile, this metformin-induced suppression of *IRF1* was abolished in SLC5A11-knockout cells ($p = 0.0091$, Fig. 3D), demonstrating the absolute requirement for SLC5A11 in this regulatory cascade.

Based on these observations, we hypothesized that IRF1, a well-characterized activator of PD-L1 transcription, functions as the key mediator of the SLC5A11-dependent regulatory axis. Immunoblot analyses demonstrated consistent metformin-induced reduction in IRF1 protein levels across all three cellular models (Fig. 3E–G). Crucially, this regulatory effect was abolished in SLC5A11-KO cells and restored upon SLC5A11 reconstitution (Fig. 3H–M), establishing the functional relationship between SLC5A11 and IRF1 protein regulation. JASPAR analysis identified 11 conserved IRF1-binding motifs of the *CD274* promoter (Supplementary Table S4). Dual-luciferase reporter assays showed that mutation of the top-predicted IRF1 binding site (from −210 to −199 bp relative to the transcription start, Supplementary Fig. S4B) significantly reduced *CD274* promoter activity compared with the wild type, indicating that IRF1 directly activates *CD274* transcription through this binding site (Fig. 3N and O). Chromatin Immunoprecipitation (ChIP) assay also confirmed that IRF1 specifically binds to this site in *CD274* promoter region (Fig. 3P). To validate these findings in vivo, immunohistochemical staining of tumor xenografts confirmed markedly attenuated IRF1 expression in metformin-treated specimens compared to vehicle controls (Fig. 3Q). Collectively, these findings delineate a previously unrecognized SLC5A11-IRF1-PD-L1 signaling axis through which metformin exerts its immunomodulatory effects.

2.5. SLC5A11-dependent metformin action regulates PD-L1 through the AMPK-JAK2-STAT1-IRF1 signaling pathway

Recent work has identified Presenilin Enhancer 2 (PEN2) as a critical interaction partner mediating metformin's biological effect through AMPK activation [19]. To examine whether PEN2 contributes to metformin-induced PD-L1 regulation, we generated PEN2-knockout U251-MG cells and assessed their response to metformin treatment (Supplementary Fig. S4C). Surprisingly, metformin retained its full capacity to suppress PD-L1 expression in PEN2-KO cells across a range of concentrations (Fig. 4A and B), demonstrating that metformin regulates PD-L1 through a PEN2-independent mechanism.

Previous studies have established AMPK activation as a central mechanism underlying metformin's ability to suppress PD-L1 expression [17]. To determine whether SLC5A11 functions upstream of this established pathway, we first assessed AMPK phosphorylation status in wild-type and SLC5A11-KO cells. Metformin treatment markedly increased AMPK phosphorylation (p-AMPK) levels in wild-type U251-MG cells, whereas this effect was abolished in SLC5A11-knockout cells (Fig. 4C and D), indicating that SLC5A11 is required for metformin-induced AMPK activation. To confirm that AMPK functions downstream of SLC5A11 in PD-L1 regulation, we found

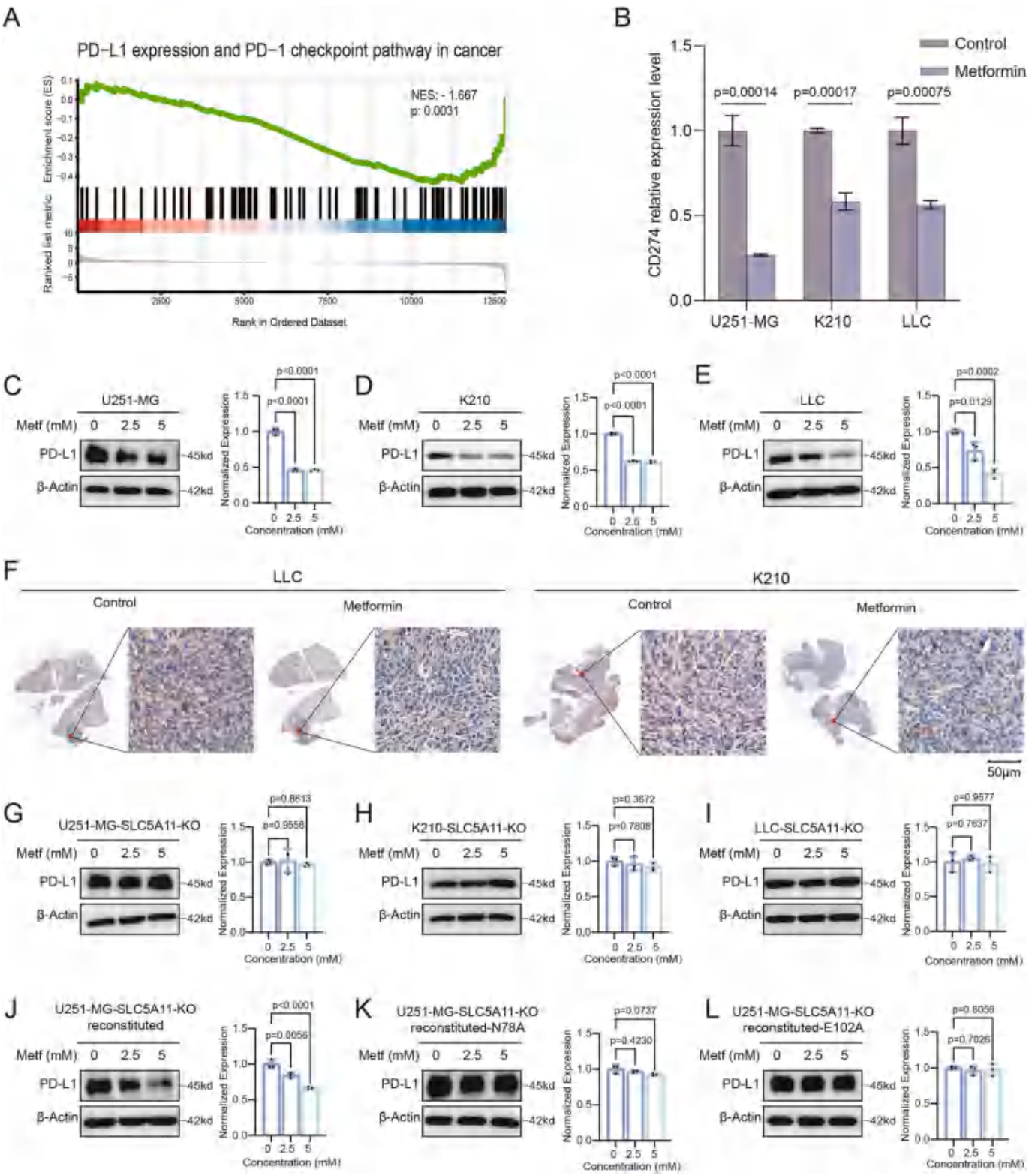

Fig. 2. Metformin down-regulates the expression of PD-L1 associated with SLC5A11

(A) Gene Set Enrichment Analysis (GSEA) of the transcriptome. (B) Quantitative RT-PCR analysis of the relative expression level of *CD274* in U251-MG, K210 and LLC cells after 5 mM metformin treatment for 72 h. (C-E) U251-MG, K210 and LLC cells were further cultured with metformin (0 mM, 2.5 mM, 5 mM) for 48 h, followed by Western blot analysis of PD-L1 expression levels. (F) Representative images of immunohistochemical staining for PD-L1 expression in LLC and K210 tumor tissues. (G-I) Stable knockout SLC5A11 in U251-MG, K210, and LLC cells, and treated these cells with 0 mM, 2.5 mM or 5 mM metformin for 48 h, followed by Western blot analysis of PD-L1 expression levels. (J-L) Reconstitution of SLC5A11 (J) or its mutant variants (K and L) in U251-MG-SLC5A11-KO cells and PD-L1 expression levels was evaluated using Western blot after metformin (0 mM, 2.5 mM, 5 mM) treatment for 48 h.

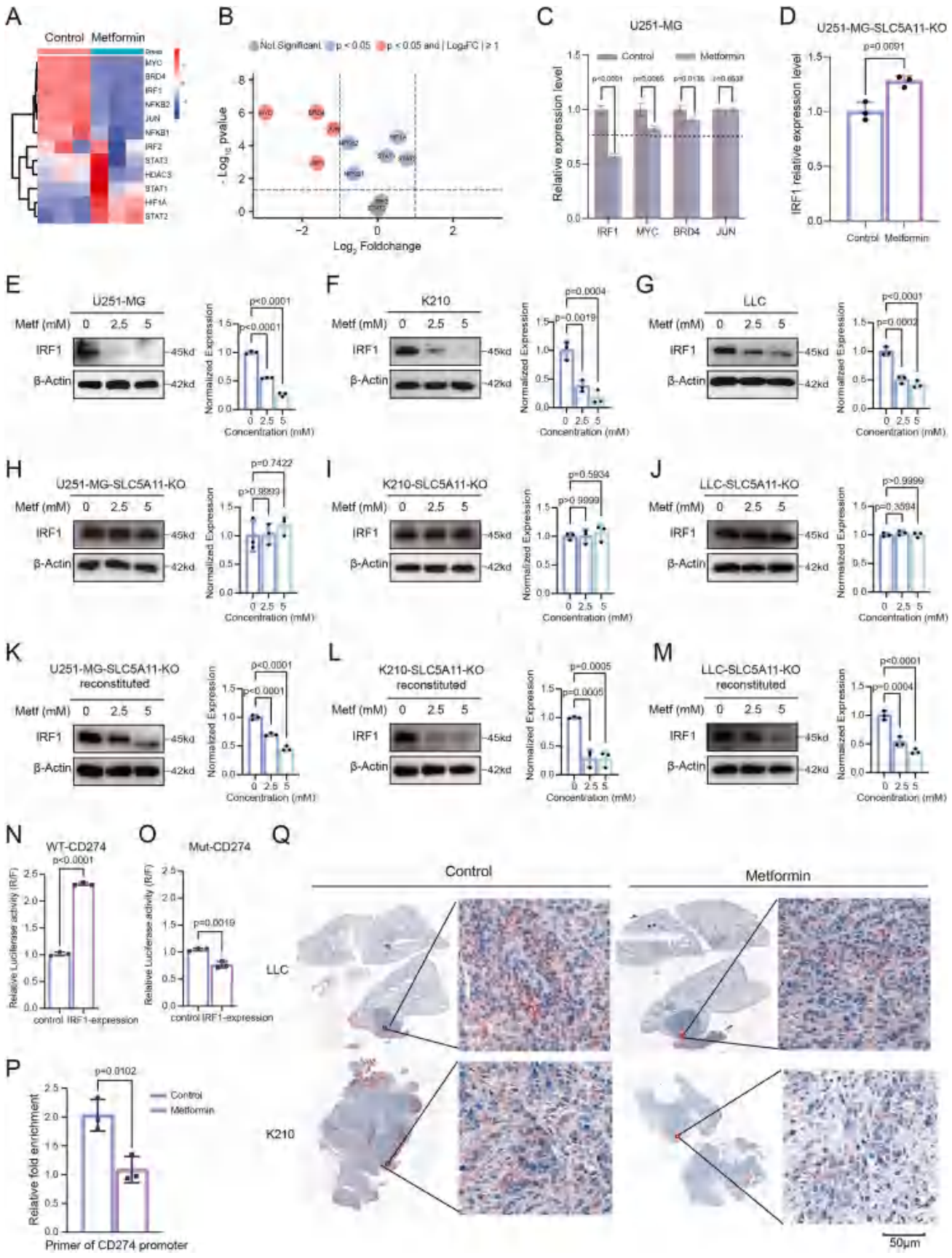

(caption on next page)

Fig. 3. Metformin represses PD-L1 transcription via IRF1-dependent mechanism
(A and B) Transcriptome data analysis of PD-L1 transcription factor expression levels: (A) Heatmap; (B) Volcano plot. (C) Quantitative RT-PCR analysis of the relative expressions level of *IRF1*, *MYC*, *BRD4* and *JUN* in U251-MG cells after 5 mM metformin treatment for 72 h. (D) Relative *IRF1* expression level of U251-MG-SLC5A11-KO cells after 5 mM metformin treatment for 72 h was analyzed by quantitative RT-PCR. (E-G) Western blot analysis of the IRF1 expression level in U251-MG, K210 and LLC cells after metformin (0 mM, 2.5 mM, 5 mM) treatment for 48 h. (H-J) Western blot analysis of the IRF1 expression level in U251-MG-SLC5A11-KO, K210-SLC5A11-KO and LLC-SLC5A11-KO cells after metformin (0 mM, 2.5 mM, 5 mM) treatment for 48 h. (K-M) Western blot analysis of the IRF1 expression level in cells with SLC5A11 reconstituted in SLC5A11-KO cells after metformin (0 mM, 2.5 mM, 5 mM) treatment for 48 h. (N) Analysis of the luciferase activity of *CD274* in U251-MG cells transfected with a wild type *CD274* promoter and a *IRF1* overexpression plasmid. (O)Analysis of the luciferase activity of *CD274* in U251-MG cells transfected with a mutant *CD274* promoter (deletion of the −210 to −199 bp relative to the transcription start of *CD274* promoter region) and a *IRF1* overexpression plasmid. (P) ChIP-qPCR detection of the binding between *IRF1* and *CD274*. (Q) Representative images of immunohistochemical staining for IRF1 expression in LLC and K210 tumor tissues.

that metformin's ability to suppress PD-L1 expression was similarly abolished upon AMPKα knockout in U251-MG cells, while SLC5A11 expression remained unaffected (Fig. 4E, Supplementary Fig. S4D). These reciprocal experiments establish that both AMPK and SLC5A11 are indispensable for metformin-induced suppression of PD-L1 expression, with SLC5A11 functioning upstream of AMPK activation.

Furthermore, we investigated whether AMPK acts through IRF1 to modulate PD-L1 expression. Our findings demonstrate that AMPK knockout completely abolished the metformin-induced reduction of IRF1 expression, establishing AMPK as an essential upstream regulator of IRF1 (Fig. 4E). To define the mechanism linking AMPK to IRF1 suppression, we examined the JAK2-STAT1 pathway, an established regulator of IRF1 transcription [22–25]. GSEA revealed significant downregulation of JAK-STAT signaling in metformin-treated cells (NES $= -1.8261$, $p = 0.0032$, Fig. 4F). Mechanistic studies demonstrated that the AMPK activator AICAR (200 μM) suppressed phosphorylation of JAK2 and STAT1, leading to decreased IRF1 and PD-L1 expression. Conversely, the AMPK inhibitor Dorsomorphin (10 μM) prevented these effects, maintaining JAK2-STAT1 activation and PD-L1 levels (Fig. 4G). These findings establish a linear signaling cascade where AMPK activation inhibits JAK2-STAT1 phosphorylation, thereby suppressing IRF1-mediated PD-L1 transcription (Fig. 4G). This newly identified SLC5A11-AMPK-JAK2-STAT1-IRF1-PD-L1 regulatory axis provides a comprehensive molecular basis for understanding how metformin enhances antitumor immunity and improves immunotherapy efficacy.

2.6. Metformin enhances immune checkpoint blockade efficacy in preclinical tumor models

To translate our mechanistic findings into a therapeutic context, we developed a luciferase-expressing Lewis lung carcinoma (LLC) orthotopic model through direct intrapulmonary injection in immune-competent mice (Fig. 5A). Following tumor establishment, mice were randomized to receive vehicle, metformin monotherapy, anti-PD1 monotherapy, or the combination of metformin plus anti-PD1. Bioluminescence imaging revealed progressive tumor growth suppression across all treatment arms relative to controls, with the combination therapy demonstrating significantly superior therapeutic efficacy (Fig. 5B–D). Quantitative analysis of tumor burden at study endpoint demonstrated 73.4% reduction in total lung weight in the combination group compared to vehicle controls (0.21 g vs 0.79 g, combination group vs control group, $p < 0.0001$), which substantially exceeded the antitumor effects observed with either metformin monotherapy (0.56 g vs 0.79 g, metformin group vs control group, $p = 0.0099$) or anti-PD1 monotherapy (0.45 g vs 0.79 g, anti-PD1 group vs control group, $p = 0.0018$) (Fig. 5B and C). The combination therapy thus exhibited synergistic rather than merely additive effects (Q = 1.20). Importantly, all treatment regimens maintained favorable safety profiles as evidenced by stable body weights throughout the study period (Δweight <5%, Supplementary Fig. S4E). This superior efficacy translated to significant survival benefit: median survival was not reached in the combination group (>60 days with 66.7% survival), compared to 29 days in controls and 36.5 - 47 days in monotherapy groups (Fig. 5E).

To translate our mechanistic findings into a therapeutic context and directly evaluate the requirement of SLC5A11 in metformin-mediated immunotherapy sensitization, we established SLC5A11 wild-type (WT) and knockout (KO) Lewis lung carcinoma (LLC) xenografts models in immune-competent mice. Consistent with our orthotopic data, combined metformin and anti-PD-1 treatment produced synergistic tumor suppression (Q = 1.16), reducing final tumor volume and tumor weight compared to vehicle controls (Fig. 5F, G and I). In contrast, this synergistic benefit was abolished in SLC5A11-KO tumors (Q = 0.96). Although anti–PD-1 monotherapy retained partial antitumor activity, the addition of metformin failed to further enhance therapeutic efficacy in the absence of SLC5A11 (Fig. 5F–H and J). These results demonstrate that tumor-intrinsic SLC5A11 expression is required for metformin to potentiate anti–PD-1 immunotherapy in vivo, thereby providing direct genetic evidence that SLC5A11 mediates the observed therapeutic synergy.

To elucidate the immunological basis for this enhanced efficacy, immunohistochemical analysis of tumor specimens revealed dramatically enhanced infiltration of $CD8^+$ cytotoxic T cells and $CD4^+$ helper T cells in the combination treatment group compared to either monotherapy (Fig. 5K). These findings suggest that metformin's ability to suppress tumor-intrinsic PD-L1 expression synergizes with systemic PD-1 blockade to overcome tumor immune evasion and enhance T cell-mediated antitumor immunity.

Given the persistent clinical challenge of immunotherapy resistance in pancreatic cancer, we next established an orthotopic pancreatic ductal adenocarcinoma (PDAC) model using luciferase-expressing K210 cells derived from LSL-Kras(G12D); Trp53 fl/fl; Pdx1-Cre mice (Fig. 6A). In this immunologically “cold” tumor model, combination therapy elicited remarkable tumor regression (0.21 g vs 0.89 g, combination group vs control group, $p < 0.0001$) significantly exceeding the effects observed with either metformin (0.68 g vs 0.89 g, metformin group vs control group, $p = 0.0428$) or anti-PD1 monotherapy (0.52 g vs 0.89 g, combination group vs control group, $p = 0.0018$) (Fig. 6B–D). The combination therapy also exhibited synergistic effects (Q = 1.38), reducing tumor burden by 3.21-fold compared to metformin treatment alone and 1.89-fold compared to anti-PD1 monotherapy. Kaplan–Meier survival analysis demonstrated that the combination therapy markedly prolonged median survival compared with the control and single-agent groups in pancreatic cancer models (>50 days with 60% survival vs. 23 days, combination group vs control group, $p < 0.0001$, Fig. 6E). Additionally, subcutaneous K210 models demonstrated remarkable sensitization to checkpoint blockade by metformin (Q = 1.21), whereas this synergistic effect was abolished following SLC5A11 knockout (Q = 0.96) (Fig. 6F–J). Consistent with the lung cancer model, immunohistochemical analysis confirmed enhanced T cell infiltration in combination-treated tumors compared to either monotherapy, without inducing weight loss or other overt toxicities (Fig. 6K, Supplementary Fig. S4F).

To establish the functional consequences of metformin-induced PD-L1 suppression, we employed ex vivo co-culture systems using human peripheral blood mononuclear cells (PBMCs). To confirm effective T cell activation, we performed flow cytometry analysis that activated T cells showed upregulation of activation markers CD69 and CD25 (Supplementary Fig. S4G). Metformin pretreatment (5 mM, 48 h) significantly enhanced tumor cell susceptibility to immune-mediated

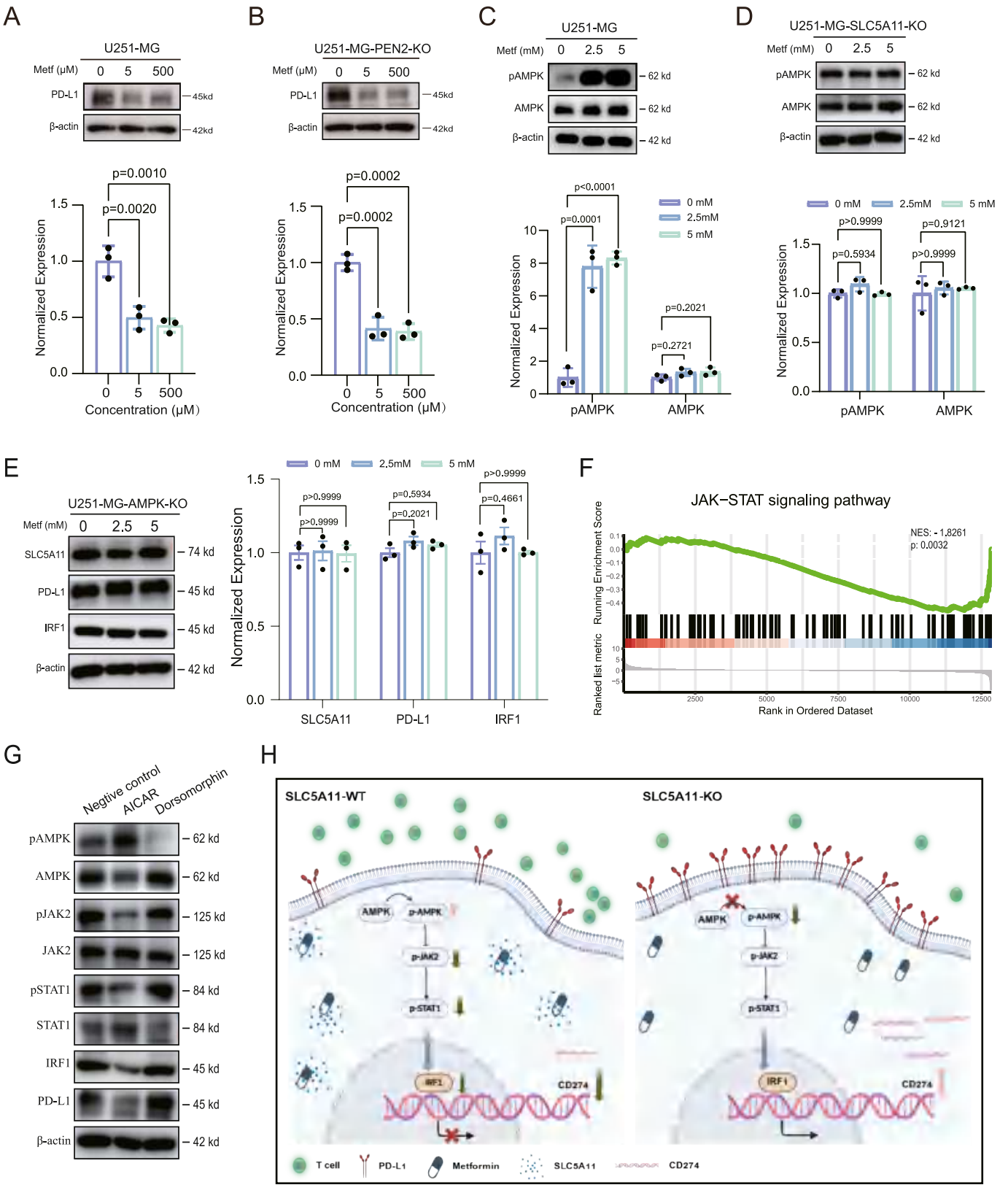

Fig. 4. SLC5A11-dependent metformin action regulates PD-L1 via AMPK-IRF1 signaling pathway
(A and B) U251-MG and U251-MG-PEN2-KO cells were cultured with low dose metformin (0, 5 μM, 500 μM) for 48 h, then PD-L1 expression levels was analyzed by Western blot. (C and D) Western blot analysis of the AMPK and p-AMPK (phosphorylation of AMPKα) expression levels in U251-MG and U251-MG-SLC5A11-KO cells after metformin (0 mM, 2.5 mM, 5 mM) treatment for 48 h. (E) Stable knockout AMPKα1 in U251-MG cells and treated with metformin, then SLC5A11, PD-L1 and IRF1 expression levels was analyzed by Western blot. (F) Gene Set Enrichment Analysis (GSEA) of transcriptomic profiles following metformin treatment. (G) Western blot analysis of the AMPK-JAK2-STAT1-IRF1-PD-L1 pathway of U251-MG cells after AMPK activators and inhibitors treatment. (H) Mechanistic diagram of metformin regulating PD-L1 expression through the SLC5A11-AMPK-IRF1 axis.

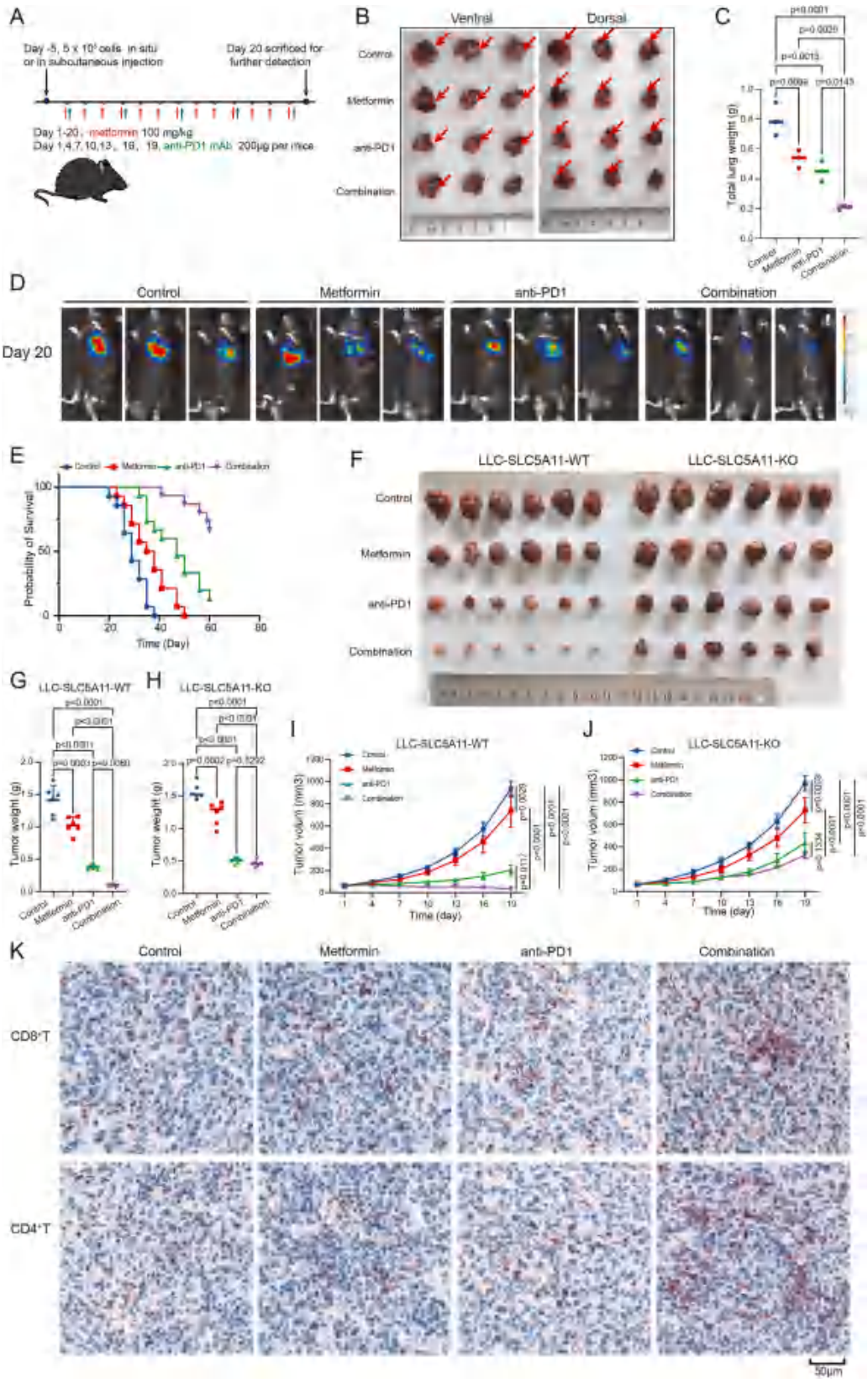

Fig. 5. Metformin enhances immune checkpoint inhibitor efficacy in lung cancer

(A) Schematic diagram of lung orthotopic tumor model construction and treatment. (B) Images of tumors after dissection (n = 3). (C) Weights of total lung after dissection. (D) Representative in vivo imaging diagrams of tumors in mice in situ. (E) Survival curve of LLC-SLC5A11-WT mouse subcutaneous tumor model (n = 15). (F) Images of subcutaneous tumors of LLC-SLC5A11-WT and LLC-SLC5A11-KO after dissection (n = 6). (G-H) Tumor weight of LLC-SLC5A11-WT (G) and LLC-SLC5A11-KO (H) subcutaneous model. (I-J) Subcutaneous tumor volume of LLC-SLC5A11-WT (I) and LLC-SLC5A11-KO (J). (K) Images of immunohistochemical staining for $CD4^+$ and $CD8^+$ T cells in tumor tissues. Results are expressed as the mean ± SD.

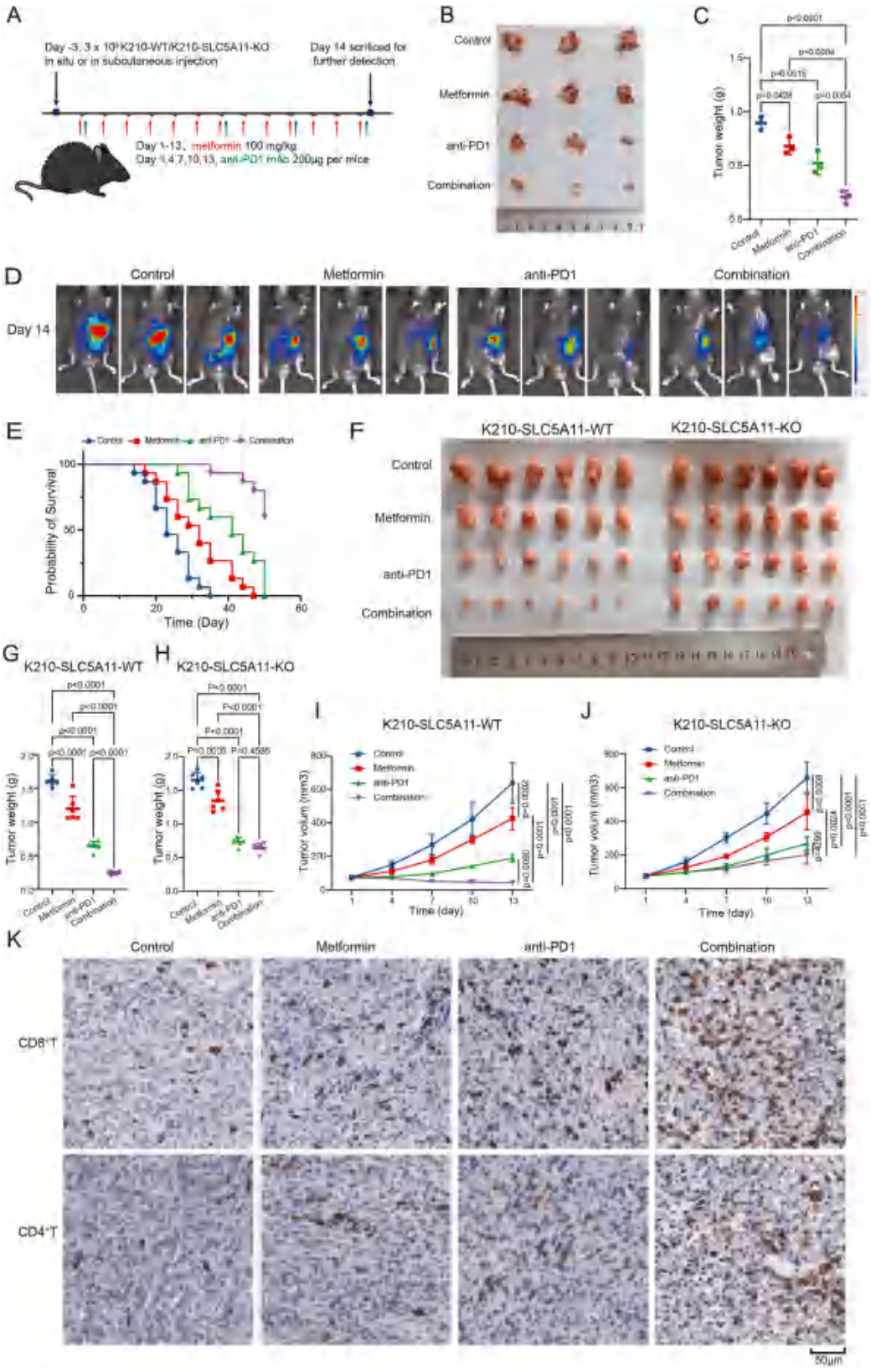

Fig. 6. Metformin enhances the efficacy of immune checkpoint inhibitor in pancreatic adenocarcinoma cancer
(A) Schematic diagram of pancreatic orthotopic tumor model construction and treatment. (B) Images of tumors after dissection (n = 3). (C) Weights of pancreatic tumor after dissection. (D) Representative in vivo imaging diagrams of tumors in mice in situ. (E) Survival curve of K210-SLC5A11-WT mouse subcutaneous tumor model (n = 15). (F) Images of subcutaneous tumors of K210-SLC5A11-WT and K210-SLC5A11-KO after dissection (n = 6). (G-H) Tumor weight of K210-SLC5A11-WT (G) and K210-SLC5A11-KO (H) subcutaneous model. (I-J) Subcutaneous tumor volume of K210-SLC5A11-WT (I) and K210-SLC5A11-KO (J). (K) Immunohistochemical staining of $CD4^+$ and $CD8^+$ T cells in tumor tissues. Results are expressed as the mean ± SD.

killing, increasing PBMC-induced apoptosis from 33.55 ± 5.48% to 45.88 ± 6.01% in U251-MG cells ($p = 0.0265$, Fig. 7A–B). However, the apoptosis level was not statistically significant in U251-MG-SLC5A11-KO cells (29.93 ± 6.75% vs. 31.67 ± 4.31%, PBMC group vs. Combination group, p = 0.9521, Fig. 7A and C). This enhanced immunogenicity was recapitulated in patient-derived pancreatic cancer organoids, where metformin pretreatment enabled effective PBMC-mediated cytotoxicity, reducing organoid viability (Fig. 7D). These findings provide direct functional evidence that metformin's modulation of tumor immune evasion mechanisms translates to enhanced susceptibility to T cell-mediated killing.

These preclinical findings provide compelling evidence that metformin enhances immune checkpoint blockade efficacy across multiple cancer types through modulation of tumor-intrinsic PD-L1 expression and consequent enhancement of T cell-mediated antitumor immunity. The synergistic effects observed in both immunologically "hot" (lung cancer) and "cold" (PDAC) tumor models underscore the broad applicability of this approach. Notably, the robust response observed in the typically immunotherapy-resistant PDAC model suggests particular promise for this combinatorial approach in enhancing the therapeutic efficacy of immune checkpoint blockade in challenging cancer types.

3. Discussion

Accumulating evidence has highlighted metformin as a potential anti-tumor agent and metformin had immunomodulatory effects in various solid tumors [5,22,23]. In this study, we have uncovered a previously unknown mechanism through which metformin modulates tumor immunity by identifying SLC5A11 as an essential mediator of metformin's immunomodulatory effects. Our comprehensive analyses

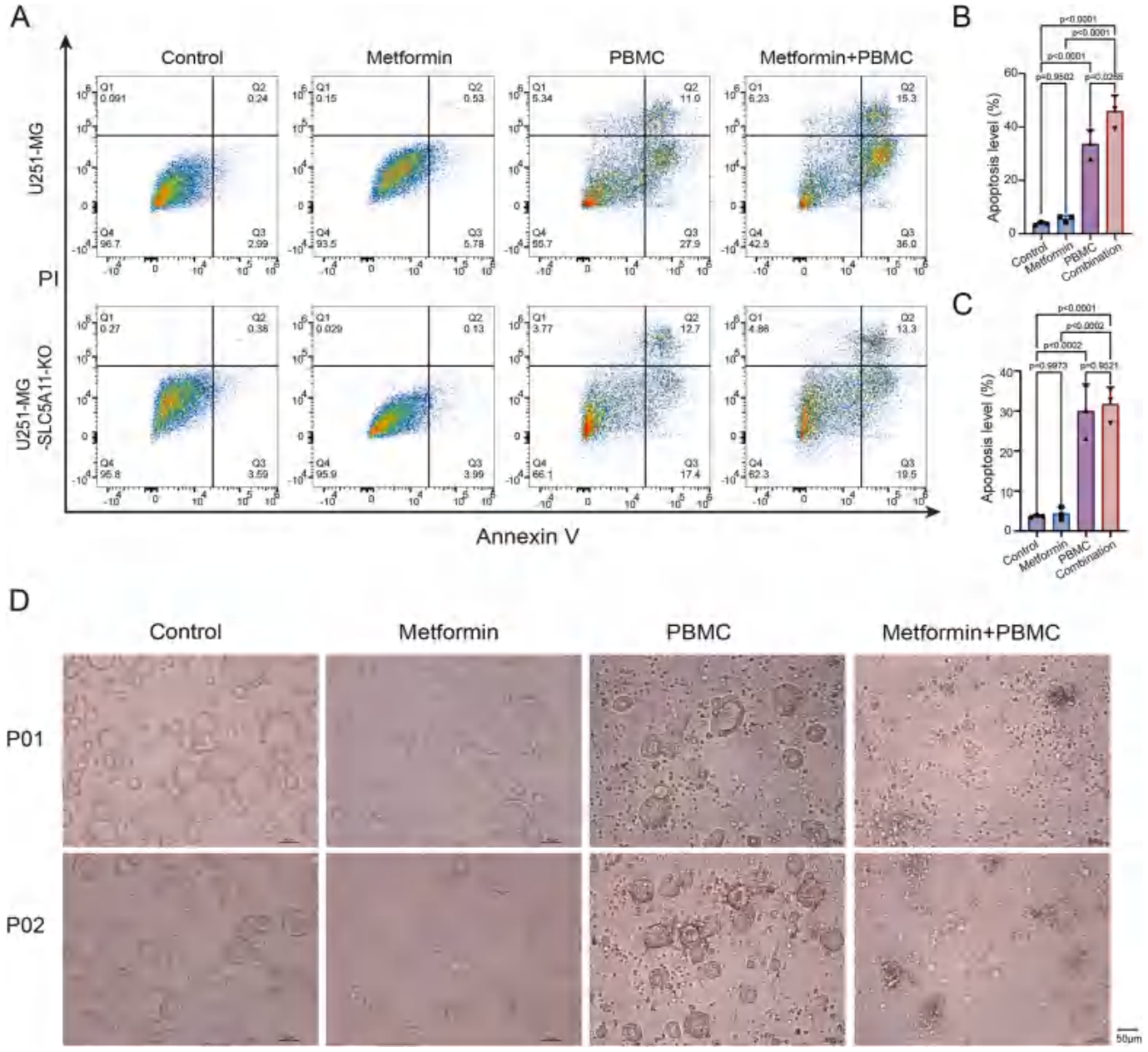

Fig. 7. Metformin enhances PBMC-mediated cytotoxicity in co-culture models
(A) Flow cytometry tests examined the apoptosis profiles of U251-MG cells and U251-MG-SLC5A11-KO cells when co-culture with PBMCs under different treatment conditions. (B-C) Quantification of the apoptosis level (Q2 + Q3) of U251-MG cells (B) and U251-MG-SLC5A11-KO cells(C) across the four treatment groups. (D) Representative images of patient-derived (P01, P02) pancreatic tumor organoids under different treatment conditions, scale bar = 50 μm.

demonstrate that metformin directly binds to SLC5A11, triggering a signaling cascade through AMPK activation and IRF1 suppression that ultimately leads to PD-L1 downregulation. These findings not only provide mechanistic insights into metformin's anticancer properties but also establishes a rational basis for combining metformin with immune checkpoint blockade therapy.

The identification of SLC5A11 as a direct target of metformin represents a significant advance in understanding metformin's pleiotropic effects. While previous studies have identified various direct targets of metformin including complex I of the mitochondrial respiratory chain [24,25], cytochrome P450 (CYP)3A4 [26], *Escherichia coli* dihydrofolate reductase (ecDHFR) [27], organic cation transporters (OCTs) [28], and more recently PEN2 [19], our work reveals SLC5A11 as a critical mediator specifically for metformin's immunomodulatory functions. The structural basis of this interaction, characterized by stable hydrogen bonding at the pocket containing Asn78 and Glu102 residues, provides a molecular framework for designing more potent immunomodulatory agents. Notably, the binding affinity between metformin and SLC5A11 exceeds that observed with other validated metformin targets, suggesting that SLC5A11 may represent a physiologically relevant target at therapeutic metformin concentrations. While structural resolution of the metformin-SLC5A11 complex awaits successful purification of this challenging membrane protein, our comprehensive functional evidence—including CETSA-demonstrated thermal stabilization, loss-of-function with binding site mutations, and SLC5A11-dependent cellular responses—strongly supports direct target engagement in the physiological membrane context. Specifically, our functional data demonstrate that metformin significantly downregulates PD-L1 expression at both the transcriptional and protein levels in multiple tumor cell lines through its interaction with SLC5A11.

Metformin is well known to activate AMPK by disrupting cellular energy homeostasis and engaging upstream kinases such as STK11 and CaMKK2 [29]. Our findings do not challenge this established paradigm, but rather identify SLC5A11 as a critical upstream determinant of metformin responsiveness. We show that loss of SLC5A11 abolishes metformin-induced AMPK activation, indicating that SLC5A11 is required for metformin to engage the canonical AMPK signaling cascade. Thus, SLC5A11 does not represent an alternative AMPK activation pathway, but instead functions upstream of the classical mechanism to enable downstream metabolic and immunomodulatory effects.

Our delineation of the SLC5A11-AMPK-PD-L1 axis reveals an elegant mechanism linking metformin cellular metabolism to immune checkpoint regulation. The linear nature of this pathway, where metformin binding to SLC5A11 leads to AMPK phosphorylation, which reduces JAK2-STAT1 phosphorylation, subsequently suppresses IRF1 to downregulate PD-L1. This mechanism complements prior reports that AMPK reduces PD-L1 through post-translational routes—such as AMPK-dependent PD-L1 phosphorylation leading to ERAD or AMPK-driven lysosomal degradation—as well as studies describing alternative AMPK-dependent transcriptional modulators of PD-L1 [17,30]. Together, these findings indicate that AMPK acts as a nodal regulator that controls PD-L1 at multiple levels: (i) post-translational modification and degradation, and (ii) transcriptional repression via distinct transcription factor axes (e.g., CEBPB family or JAK2–STAT1–IRF1) [17,30–34]. Although AMPK is a Ser/Thr kinase, its activation can suppress JAK–STAT signaling through indirect mechanisms, leading to a net reduction in tyrosine phosphorylation of JAK2 and STAT1. Previous studies have shown that AMPK can negatively regulate JAK family kinases [35–37]. Activation of AMPK has been shown to activates phosphatases (e.g., PP2A) and suppresses positive regulators (e.g., SHP-2), resulting in secondary loss of JAK2 tyrosine phosphorylation [38]. In addition, AMPK can inhibit JAK signaling by phosphorylating non-catalytic serine residues on JAK family members or associated regulatory proteins, thereby impairing kinase activity or promoting inhibitory protein interactions (e.g., 14-3-3 binding) [36]. Consistent with these reports, our data support a model in which AMPK activation negatively regulates JAK2–STAT1 signaling, thereby reducing IRF1-dependent PD-L1 transcription. This mechanism is compatible with, and does not contradict, the established role of AMPK as a kinase.

This finding has important implications for therapeutic targeting, as it identifies multiple nodes for intervention. The PEN2-independence of this pathway is particularly intriguing, suggesting that metformin's effects on lysosomal AMPK activation [19] and immune checkpoint regulation represent distinct mechanisms that may synergize in vivo. Key mechanistic questions remain to be addressed. First, determining whether SLC5A11 is essential for all AMPK-mediated PD-L1 regulation—including post-translational phosphorylation and ERAD—will establish the full scope of this regulatory axis. Second, systematic analysis of crosstalk between the JAK2-STAT1-IRF1 pathway and other AMPK-responsive transcriptional networks (CEBPB) may reveal synergistic regulatory nodes for therapeutic exploitation. Such studies will inform whether targeting SLC5A11 alone is sufficient or whether multi-pathway modulation is necessary for optimal immunotherapeutic outcomes. The transcriptional regulation of PD-L1 through IRF1 adds another layer to our understanding of immune checkpoint control. While multiple transcription factors including NF-κB, STAT3, HIF-1α, and MYC have been implicated in PD-L1 regulation [39–42], our findings position IRF1 as a critical mediator downstream of metabolic signals. The AMPK-dependent suppression of IRF1 through JAK2-STAT1 pathway suggests a previously unappreciated link between cellular energy status and interferon signaling pathways. Although STAT1 has been reported to directly regulate PD-L1 transcription, STAT1-dependent PD-L1 expression is not limited to direct STAT1 binding and, in many biological contexts, is predominantly mediated through induction of IRF1, a well-established downstream transcriptional effector of STAT1 signaling [43,44]. Consistent with this hierarchy, our data identify IRF1 as a key transcriptional mediator linking SLC5A11–AMPK signaling to PD-L1 regulation. This connection may have evolved as a mechanism to coordinate metabolic stress responses with immune regulation, potentially explaining why metabolically stressed tumor cells often exhibit altered immunogenicity.

From a translational perspective, our findings provide strong rationale for repurposing metformin as an immunomodulatory adjuvant in cancer therapy. PD-L1 expression is the only Food and Drug Administration-approved predictive biomarker for non-small cell lung cancer (NSCLC) [45]. Inhibition of PD-L1 could enhance anti-tumor immunity [46–48]. The synergistic effects observed in both immunologically “hot” (lung cancer) and “cold” (pancreatic cancer) tumor models suggest broad applicability across cancer types. The ability of metformin to convert immunologically cold tumors into T cell-inflamed environments is particularly exciting given the limited success of checkpoint inhibitors in such cancers. Moreover, the favorable safety profile of metformin, combined with its oral bioavailability and low cost, makes it an attractive candidate for combination immunotherapy strategies.

In conclusion, our identification of the SLC5A11-AMPK-PD-L1 axis fundamentally advances our understanding of how metabolic interventions can reshape tumor immunity. This work not only provides mechanistic insights into metformin's anticancer effects but also establishes a paradigm for rationally combining metabolic modulators with immunotherapy.

4. Materials and methods

4.1. Materials

Metformin (HY-B0627), AICAR (HY-13417) and Dorsomorphin (HY-13418A) were purchased from MedChemExpress (Beijing, China). CY5-Metformin (Q-0831396) was purchased from Xi'an ruixi Biological Technology Co., Ltd (Xi’An, China). InVivoMAb anti-mouse PD-1 (BE0273) was purchased from BioXCell (America).

4.2. Cell lines

The U251-MG cell (from the National Infrastructure of Cell Line Resource, Beijing, China), K210 cell (isolated from the spontaneous pancreatic ductal adenocarcinoma of C57BL/6J LSL-Kras(G12D); Trp53 fl/fl; Pdx1-Cre mice) and Lewis lung carcinoma cell (LLC, from the National Infrastructure of Cell Line Resource, Beijing, China) were cultured in DMEM (Gibco) supplemented with 10 % fetal bovine serum (FBS, Cell, China) and 1% penicillin-streptomycin (Gibco). All cells were incubated at 37 °C with 5% CO_2.

4.3. Genome-wide CRISPR/Cas9 screen

Genome-wide CRISPR/Cas9 knockout library (Brunello) infected U251-MG cells with 500-fold coverage and with a low multiplicity of infection (MOI <0.3). After 48 h of puromycin selection, the cells were divided into two groups. The treatment group and control group were following a 14 days incubation with or without metformin. Then, genomic DNA was extracted and the sgRNA fragment was amplified through two rounds of PCR to construct a sequencing library. SgRNA abundance was sequenced on a HiSeq X10 platform (Illumina; San Diego, CA, USA) and analyzed by MAGeCK algorithm [49].

4.4. Molecular docking

The SDF format ligand file of metformin was obtained from the PubChem database (https://pubchem.ncbi.nlm.nih.gov/), and the three-dimensional structure models of the SLC5A11 protein was obtained from the UniProt database (https://www.uniprot.org/). AutoDockTools 1.5.6 was used to convert ligand and receptor files to pdbqt format and improve their structure by replacing water molecules with hydrogen atoms. Molecular docking was conducted using AutoDock Vina 1.2.5, and PyMOL 2.4.0 was used for further analysis and visualization.

4.5. Molecular dynamics simulation

Molecular dynamics (MD) simulations on the conformations that ranked first in each of the three regions were performed using GROMACS 2024.3 software. The AMBER99SB force field and SPC water model were used, and the system temperature was 300 K and the simulation time was 100 ns. The steepest descent method was applied for energy minimization, followed by equilibration to stabilize the system prior to conducting the MD simulation. The binding free energies were calculated using the MM/GBSA method.

4.6. Cellular thermal shift assay (CETSA)

The core of the CETSA is to verify the direct interaction between a drug and its target protein by detecting changes in the thermal stability of the protein following binding. U251-MG cells were seeded into 10 cm dishes and cultured to the logarithmic growth phase, then divided into a negative control group and a metformin-treated group (5 mM) for 2 h of incubation. After incubation, the cells were harvested and counted. For each group, 2×10^7 cells were taken, equally divided into 8 PCR tubes, and resuspended in PBS containing PMSF. The cells in the PCR tubes were subjected to gradient heating at 37 °C, 42 °C, 47 °C, 52 °C, 57 °C, 62 °C, 67 °C, and 72 °C respectively. Each tube was heated for 3 min, placed at room temperature for another 3 min, and then transferred to ice. After all heating steps were completed, the cells were repeatedly freeze-thawed 3 times using liquid nitrogen. Subsequently, centrifugation was performed at 12,000 rpm and 4 °C for 20 min. The supernatant was collected, mixed with 6 × protein loading buffer, heated at 100 °C for 5 min, and then subjected to Western blot to detect the expression of SLC5A11 protein [50,51].

4.7. Cell viability assay

U251-MG cells were seeded into 96-well plates and cultured overnight, then switched to a medium containing different concentrations of metformin. After 48 h of incubation, the absorbance of the cells was determined using the CCK8 kit (MA0218, Meilunbio, China). GraphPad Prism was used to calculate cell viability and plot growth curves.

4.8. RNA sequencing and data analysis

U251-MG cells were seeded into 6-well plates and cultured overnight, then cells were treated with 5 mM metformin or PBS for 72 h. Cells were collected and total RNA was isolated using an RNA-quick purification kit (ES Science, Shanghai, China). Then RNA sequencing (Illumina HiSeq system) was performed and preliminary analyzed by Tsingke Biotech company (Beijing, China). DESeq2 was used for differential gene analysis. The Gene Set Enrichment Analysis (GSEA) was performed by GSEA v4.2.

4.9. Lentivirus production and transduction (gene knockout and overexpression)

The lentiCRISPR v2 system was used for gene knockout. Single-guide RNA (sgRNA) sequences (see Table S5 for detailed sequences) were designed and ligated into the lentiCRISPR v2 vector to construct recombinant knockout plasmids. The overexpression plasmids, including pLV3-CMV-Slc5a11(mouse)-3 × FLAG-CopGFP-Neo plasmid and pLV3-CMV-SLC5A11(human)-3 × FLAG-EF1a-CopGFP-Neo plasmid were purchased from MiaoLing Plasmid Platform. Lentivirus production was conducted by transfecting these plasmids into HEK293T cells (along with packaging plasmids psPAX2 and pMD2.G), and the lentivirus-containing supernatants were collected. Infect cells with lentivirus and select with puromycin or neomycin.

4.10. Chromatin immunoprecipitation (ChIP)-qPCR assay

Chromatin Immunoprecipitation Assay Kit (#17-295, Millipore) was used for chromatin immunoprecipitation assay. U251-MG cells were pretreated with 5 mM metformin or PBS. A total of 1×10^6 cells were used for each ChIP assay. Sonication was carried out in 50W mode with a 2 mm ultrasonic probe, set at 30% of the maximum power. Under ice-cold conditions, the sonication process was performed with cycles of 20 s of sonication followed by 30 s of rest, repeated 7 times. Agarose gel electrophoresis confirmed that this sonication protocol yielded DNA fragments of roughly 200-300 bp in length. IRF1 antibody (Invitrogen, PA5-147374) and corresponding isotype control were added into the prewashed sample. DNA fragments were recovered using DNA Clean & Concentrator KIT (#D4013, ZYMO) and verified by RT-qPCR. Specific primers are shown in Table S5. Results were normalized to input DNA and are presented as relative enrichment.

4.11. Dual-luciferase reporter assays

U251-MG cells (1.5×10^5 per well) were seeded into 6-well plates and cultured until they reached approximately 70–80% confluence. Cells were then co-transfected with a pCMV-IRF1 expression plasmid or control vector, a Renilla luciferase control plasmid, and either a wild-type (WT) or IRF1-binding–site mutant (Mut) *CD274* promoter–luciferase reporter construct. After 24 h, cell lysates were prepared using the Dual-Luciferase® Reporter Assay System (Promega, Cat. E1910). Firefly luciferase activity driven by the *CD274* promoter was normalized to Renilla luciferase activity.

4.12. Quantitative real-time PCR

Total RNA was isolated using an RNA-quick purification kit (ES-

RN001, ES Science, Shanghai, China) and reverse transcription using the PrimeScript™ RT Master Mix (RR036A, Takara, Tokyo, Japan). Then, qRT-PCR was performed using TB Green® Premix Ex Taq™ (RR420A, Takara, Tokyo, Japan). Finally, the quantification of gene expression was normalized to β-actin and analyzed using the $2^{-\Delta\Delta CT}$ method. The primer sequences used are shown in Table S5.

4.13. Western blot

Cells were lysed by protein lysis buffer. Using the BCA kit to determine the concentration of the extracted protein. Equal amounts of protein lysate (30 μg) were separated by SDS-PAGE gel and electrotransferred onto a PVDF membrane (Millipore). After blocking with 5% milk in TBST, the membrane was incubated with primary antibodies overnight at 4 °C and HRP-conjugated secondary antibodies 1 h at room temperature. Imaged using a chemiluminescence imager and quantified with ImageJ.

4.14. Animal experiments

C57BL/6 mice (6-8 weeks, male) were purchased from Beijing Huafukang Biological Technology Co., Ltd. (Beijing, China). All mice were housed in a specific pathogen–free animal facility with individually ventilated cages (IVCs).

For the construction of orthotopic lung cancer model, 5×10^5 LLC-OVA-Luc cells were injected into the lung of the C57/BL6J mice. For the construction of pancreatic orthotopic cancer model, 3×10^5 K210-OVA-Luc cells were injected into the pancreas of the C57/BL6J mice. For the construction of subcutaneous tumor models, 5×10^5 LLC-SLC5A11-WT or LLC-SLC5A11-KO cells or 3×10^5 K210-SLC5A11-WT or K210-SLC5A11-KO cells were inoculated into the right axilla of mice. At the beginning of treatment, tumor-bearing mice were randomly divided into four groups: vehicle, metformin monotherapy, anti-PD1 monotherapy, or the combination of metformin plus anti-PD1. Metformin (100 mg/kg) was administered daily by gavage. Anti-PD1 (200 μg per mouse) was administered by intraperitoneal injection every 3 days. Mouse body weights and tumor volume (subcutaneous tumor) were measured every 3 days. Quantitative bioluminescence imaging was used to reflect tumor burden.

Jin's formula was used to evaluate the combination effect of metformin and anti-PD1. The formula is $Q = E(A+B)/(EA + EB - EA \times EB)$. Specifically, Q is the combination index, E (A + B) is the inhibition rate of the combined therapy, and EA, EB is the inhibition rate of metformin and anti-PD1, respectively. The classification of Q value is as follows: $Q < 0.85$ is an antagonistic effect; $0.85 \leq Q < 1.15$ is an additive effect; $Q \geq 1.15$ is a synergistic effect. Tumor weight was used to evaluate the treatment efficacy, it was calculated as follows: [1-Treatment/Vehicle] × 100% [52].

4.15. Immunohistochemistry

For immunohistochemistry (IHC) analysis staining, paraffin-embedded tissues were cut into 5 μm sections. The sections were deparaffinized in xylene and rehydrated through a graded ethanol series and then subjected to antigen repair with the microwave boiling method. Endogenous peroxidase activity was blocked by incubation with 3% hydrogen peroxide at room temperature for 10 min. Then, the slides were incubated with anti-CD4 (ab183685, abcam), anti-CD8α (ab217344, abcam), anti-PD-L1 (NBP1-76769, Novus) or anti-IRF1 (8478T, CST) antibody overnight at 4 °C. The next day, secondary antibody was applied for 60 min at room temperature, and color was developed with a diaminobenzidine peroxidase substrate kit (ZLI-9018) or AEC Peroxidase Substrate Kit (Vector Laboratories, SK-4200). Sections were then counterstained with hematoxylin, dehydrated and mounted.

4.16. Co-culture experimental

Peripheral blood mononuclear cells (PBMCs) were obtained by Milecell Biological Science & Technology Co.,Ltd. T-cell activation was carried out using anti-CD3/CD28 antibodies in the presence of interleukin-2 (IL-2, 200 IU/mL). For co-culture assays, tumor cells and PBMCs were seeded in 6-well plates at a 1:2 ratio. After 48 h of co-culture, all cells in each well were harvested for flow cytometry analysis. Tumor cells were distinguished from immune cells by CD45 staining, followed by Annexin V-FITC/PI double staining to assess tumor cell apoptosis. Flow cytometry data were analyzed with FlowJo software. For co-culture experiments involving pancreatic cancer organoids, the wells of 96-well plates were pre-coated with 10% Matrigel prior to organoid seeding. Organoids and PBMCs were then co-cultured at a 1:4 ratio. After 48 h, bright-field images were captured using an inverted microscope to monitor organoid morphology and viability.

4.17. Statistical analysis

All statistical analyses were performed using GraphPad Prism 10. Graphed data represent the means ± standard deviation from at least three independent experiments. One-way analysis of variance (one-way ANOVA) is adopted for multiple group data comparison, and two-tailed, unpaired Student's t-test is used for two group data comparison.

CRediT authorship contribution statement

Yarui Ma: Writing – review & editing, Writing – original draft, Supervision, Methodology, Investigation, Funding acquisition, Data curation, Conceptualization. **Xue Wang:** Writing – original draft, Visualization, Methodology, Investigation, Formal analysis, Data curation. **Zhewen Wei:** Writing – original draft, Validation, Resources, Methodology, Investigation. **Qi Zhang:** Visualization, Methodology, Formal analysis. **Fangqing Yuan:** Methodology, Investigation. **Chungui Xu:** Methodology, Formal analysis. **Chang Liu:** Software, Formal analysis. **Xiaobing Wang:** Writing – review & editing, Supervision, Project administration, Methodology, Conceptualization. **Lin Li:** Writing – review & editing, Supervision, Project administration, Conceptualization. **Yuchen Jiao:** Writing – review & editing, Supervision, Project administration, Funding acquisition, Conceptualization.

Ethics statement

All animal experiments were approved by and performed according to the animal ethical committee at the Cancer Hospital, Chinese Academy of Medical Sciences (NCC2025A086). PBMCs used in this study were obtained from Mile-stone Biological Science & Technology Co., Ltd. (Shanghai, China). All procedures involving human PBMCs were approved by the Ethics Committee of Shanghai Liquan Hospital (Approval No. X-LQ-SHSLT-23-10-001). The patient-derived tumor organoids experiments were approved by ethics committee of National Cancer Center/Cancer Hospital, ChineseAcademy of Medical Sciences and Peking Union Medical College (24/001-4281).

Declaration of competing interest

The authors declare that they have no known competing financial interests or personal relationships that could have appeared to influence the work reported in this paper.

Acknowledgements

The project is supported by Noncommunicable Chronic Disease-National Science and Techology Major Project (2024ZD0533300), National Natural Science Foundation fund (82302943, 82225033, U24A6012, 82372696), Young Elite Scientists Sponsorship Program by

CAST (2023QNRC001), the China Postdoctoral Science Foundation (2023M730326, 2024T170073), Postdoctoral Fellowship Program of China Postdoctoral Science Foundation (GZB20230082), the Special Research Fund for Central Universities, Peking Union Medical College (3332023030), the Chinese Academy of Medical Sciences (CAMS) Innovation Fund for Medical Sciences (CIFMS) (2021-I2M-1-067, 2023-I2M-2-004, 2025-I2M-FGS-002), Shenzhen Medical Research Fund (C2401004).

Appendix A. Supplementary data

Supplementary data to this article can be found online at https://doi.org/10.1016/j.canlet.2026.218311.

References

[1] L. O'Connor, et al., Association of metformin use and cancer incidence: a systematic review and meta-analysis, J. Natl. Cancer Inst. 116 (4) (2024) 518–529.
[2] C. Coyle, et al., Metformin as an adjuvant treatment for cancer: a systematic review and meta-analysis, Ann. Oncol. 27 (12) (2016) 2184–2195.
[3] M. Foretz, et al., Metformin: from mechanisms of action to therapies, Cell Metab. 20 (6) (2014) 953–966.
[4] V. Finisguerra, et al., Metformin improves cancer immunotherapy by directly rescuing tumor-infiltrating CD8 T lymphocytes from hypoxia-induced immunosuppression, J. Immunother. Cancer 11 (5) (2023).
[5] X. Huang, et al., Metformin reprograms tryptophan metabolism to stimulate CD8+ T-cell function in colorectal cancer, Cancer Res. 83 (14) (2023) 2358–2371.
[6] Y. Kunisada, et al., Attenuation of CD4(+)CD25(+) regulatory T cells in the tumor microenvironment by metformin, a type 2 diabetes drug, EBioMedicine 25 (2017) 154–164.
[7] G.G. Chen, et al., Impact of metformin on immunological markers: implication in its anti-tumor mechanism, Pharmacol. Ther. 213 (2020) 107585.
[8] J. Panaampon, Y. Zhou, C. Saengboonmee, Metformin as a booster of cancer immunotherapy, Int. Immunopharmacol. 121 (2023) 110528.
[9] S. Wabitsch, et al., Metformin treatment rescues CD8(+) T-cell response to immune checkpoint inhibitor therapy in mice with NAFLD, J. Hepatol. 77 (3) (2022) 748–760.
[10] J. Liu, et al., Metformin-based nanomedicines for reprogramming tumor immune microenvironment, Theranostics 15 (3) (2025) 993–1016.
[11] M. Dus, M. Ai, G.S. Suh, Taste-independent nutrient selection is mediated by a brain-specific Na+/solute co-transporter in Drosophila, Nat. Neurosci. 16 (5) (2013) 526–528.
[12] L. Schaller, V.M. Lauschke, The genetic landscape of the human solute carrier (SLC) transporter superfamily, Hum. Genet. 138 (11-12) (2019) 1359–1377.
[13] K. Rashid, et al., Solute carriers as potential oncodrivers or suppressors: their key functions in malignant tumor formation, Drug Discov. Today 26 (7) (2021) 1689–1701.
[14] Y. Zhang, et al., The SLC transporter in nutrient and metabolic sensing, regulation, and drug development, J. Mol. Cell Biol. 11 (1) (2019) 1–13.
[15] V.L. Payen, et al., Monocarboxylate transporter MCT1 promotes tumor metastasis independently of its activity as a lactate transporter, Cancer Res. 77 (20) (2017) 5591–5601.
[16] K. Sun, et al., Oxidized ATM-mediated glycolysis enhancement in breast cancer-associated fibroblasts contributes to tumor invasion through lactate as metabolic coupling, EBioMedicine 41 (2019) 370–383.
[17] J.H. Cha, et al., Metformin promotes antitumor immunity via endoplasmic-reticulum-associated degradation of PD-L1, Mol. Cell 71 (4) (2018) 606–620.e7.
[18] L.E. Munoz, et al., Metformin reduces PD-L1 on tumor cells and enhances the anti-tumor immune response generated by vaccine immunotherapy, J. Immunother. Cancer 9 (11) (2021).
[19] T. Ma, et al., Low-dose metformin targets the lysosomal AMPK pathway through PEN2, Nature 603 (7899) (2022) 159–165.
[20] L. Yao, et al., The direct targets of metformin in diabetes and beyond, Trends Endocrinol. Metabol. 36 (4) (2025) 364–372.
[21] M. Yi, et al., Regulation of PD-L1 expression in the tumor microenvironment, J. Hematol. Oncol. 14 (1) (2021) 10.
[22] S. Eikawa, et al., Immune-mediated antitumor effect by type 2 diabetes drug, metformin, Proc. Natl. Acad. Sci. U. S. A. 112 (6) (2015) 1809–1814.
[23] D.L. Almeida-Nunes, et al., Enhancing immunotherapy in ovarian cancer: the emerging role of metformin and statins, Int. J. Mol. Sci. 25 (1) (2023).
[24] Z. Drahota, et al., Biguanides inhibit complex I, II and IV of rat liver mitochondria and modify their functional properties, Physiol. Res. 63 (1) (2014) 1–11.
[25] M.J. Spiering, The mystery of metformin, J. Biol. Chem. 294 (17) (2019) 6689–6691.
[26] Z. Guo, et al., Heme binding biguanides target cytochrome P450-Dependent cancer cell Mitochondria, Cell Chem. Biol. 24 (10) (2017) 1314.
[27] S.A. Gabel, et al., A structural basis for biguanide activity, Biochemistry 56 (36) (2017) 4786–4798.
[28] G.G. Graham, et al., Clinical pharmacokinetics of metformin, Clin. Pharmacokinet. 50 (2) (2011) 81–98.
[29] J. Kim, et al., AMPK activators: mechanisms of action and physiological activities, Exp. Mol. Med. 48 (4) (2016) e224.
[30] B. Liu, et al., Platinum-Metformin conjugates acting as promising PD-L1 inhibitors through the AMP-Activated protein kinase mediated lysosomal degradation pathway, Angew Chem. Int. Ed. Engl. 63 (49) (2024) e202410586.
[31] S.H. Park, et al., Metformin suppresses both PD-L1 expression in cancer cells and cancer-induced PD-1 expression in immune cells to promote antitumor immunity, Ann Lab Med 44 (5) (2024) 426–436.
[32] J. Xue, et al., Metformin suppresses cancer cell growth in endometrial carcinoma by inhibiting PD-L1, Eur. J. Pharmacol. 859 (2019) 172541.
[33] B. Chen, et al., DENR controls JAK2 translation to induce PD-L1 expression for tumor immune evasion, Nat. Commun. 13 (1) (2022) 2059.
[34] T. Lu, et al., Metformin inhibits human non-small cell lung cancer by regulating AMPK-CEBPB-PDL1 signaling pathway, Cancer Immunol. Immunother. 71 (7) (2022) 1733–1746.
[35] C. Speirs, et al., Linking energy sensing to suppression of JAK-STAT signalling: a potential route for repurposing AMPK activators? Pharmacol. Res. 128 (2018) 88–100.
[36] C. Rutherford, et al., Phosphorylation of Janus kinase 1 (JAK1) by AMP-activated protein kinase (AMPK) links energy sensing to anti-inflammatory signaling, Sci. Signal. 9 (453) (2016) ra109.
[37] S.J. Mancini, et al., Activation of AMP-activated protein kinase rapidly suppresses multiple pro-inflammatory pathways in adipocytes including IL-1 receptor-associated kinase-4 phosphorylation, Mol. Cell. Endocrinol. 440 (2017) 44–56.
[38] I. Kawashima, K. Kirito, Metformin inhibits JAK2V617F activity in MPN cells by activating AMPK and PP2A complexes containing the B56α subunit, Exp. Hematol. 44 (12) (2016) 1156–1165.e4.
[39] V. Atsaves, et al., PD-L1 is commonly expressed and transcriptionally regulated by STAT3 and MYC in ALK-negative anaplastic large-cell lymphoma, Leukemia 31 (7) (2017) 1633–1637.
[40] L. Du, et al., beta-Catenin induces transcriptional expression of PD-L1 to promote glioblastoma immune evasion, J. Exp. Med. 217 (11) (2020).
[41] H.J. Janse van Rensburg, et al., The Hippo pathway component TAZ promotes immune evasion in human cancer through PD-L1, Cancer Res. 78 (6) (2018) 1457–1470.
[42] E. Papalexi, et al., Characterizing the molecular regulation of inhibitory immune checkpoints with multimodal single-cell screens, Nat. Genet. 53 (3) (2021) 322–331.
[43] J.W. Moon, et al., IFNγ induces PD-L1 overexpression by JAK2/STAT1/IRF-1 signaling in EBV-positive gastric carcinoma, Sci. Rep. 7 (1) (2017) 17810.
[44] N. Blazanin, et al., Activation of a protumorigenic IFNγ/STAT1/IRF-1 signaling pathway in keratinocytes following exposure to solar ultraviolet light, Mol. Carcinog. 58 (9) (2019) 1656–1669.
[45] H. Rizvi, et al., Molecular determinants of response to anti-programmed cell death (PD)-1 and anti-programmed death-ligand 1 (PD-L1) blockade in patients with non-small-cell lung cancer profiled with targeted next-generation sequencing, J. Clin. Oncol. 36 (7) (2018) 633–641.
[46] H. Yao, et al., Inhibiting PD-L1 palmitoylation enhances T-cell immune responses against tumours, Nat. Biomed. Eng. 3 (4) (2019) 306–317.
[47] S. Li, et al., m(1)A inhibition fuels oncolytic virus-elicited antitumor immunity via downregulating MYC/PD-L1 signaling, Int. J. Oral Sci. 16 (1) (2024) 36.
[48] J. Dai, et al., Deep downregulation of PD-L1 by caged peptide-conjugated AIEgen/miR-140 nanoparticles for enhanced immunotherapy, Angew Chem. Int. Ed. Engl. 61 (18) (2022) e202117798.
[49] Y. Ma, et al., A CRISPR knockout negative screen reveals synergy between CDKs inhibitor and metformin in the treatment of human cancer in vitro and in vivo, Signal Transduct. Targeted Ther. 5 (1) (2020) 152.
[50] D. Martinez Molina, et al., Monitoring drug target engagement in cells and tissues using the cellular thermal shift assay, Science 341 (6141) (2013) 84–87.
[51] R. Jafari, et al., The cellular thermal shift assay for evaluating drug target interactions in cells, Nat. Protoc. 9 (9) (2014) 2100–2122.
[52] L. Xie, et al., Securinine inhibits the tumor growth of human bladder cancer cells by suppressing Wnt/β-catenin signaling pathway and activating p38 and JNK signaling pathways, Biochem. Pharmacol. 223 (2024) 116125.